Oil Shale, 2019, Vol. 36, No. 4, pp. 462–482
doi: https://doi.org/10.3176/oil.2019.4.02
ISSN 0208-189X

Kinetic study on the pyrolysis behavior of Jimsar oil shale

Ni Pan, Danni Li, Wei Lü, Fangqin Dai*

Key Laboratory for Ferrous Metallurgy and Resources Utilization of Ministry of Education, Wuhan University of Science and Technology, No. 947 Heping Avenue, Qingshan District, Wuhan 430081, PR China

Abstract. *It is well known that the process of oil shale pyrolysis is extremely complicated, for several competing or parallel reactions occur simultaneously, and various products are continuously generated, serving as new reactants. In this work, it is assumed that there occur two parallel reactions in the devolatilization of organic matter, one represents the volatilization of bitumen and the other represents the pyrolysis of kerogen. Kinetic triplets for the competing or parallel reactions are different from each other. To investigate the pyrolysis mechanism of Jimsar oil shale of Xinjiang Province, China in more detail, the bi-Gaussian distribution method, a multi-stage parallel reaction model and two master plots methods are adopted to determine the kinetic models in this work. The apparent activation energy (E) is calculated by the Flynn-Wall-Ozawa (F-W-O), Kissinger-Akahira-Sunose (K-A-S) and Friedman methods. According to the results, it can be concluded that heating rate exerts little influence on the kinetic parameters but has some impact on the pyrolysis process as a whole. The results of this work reveal the pyrolysis characteristics of oil shale to a certain extent.*

Keywords: *Jimsar oil shale, pyrolysis mechanism, master plots method, activation energy.*

1. Introduction

Due to the finite reserves of conventional fossil fuels and increasing demand for energy resource, oil shale has been paid more and more attention as an alternative energy source in recent times. In order to obtain shale oil gas, liquid and solid products from oil shale, pyrolysis is almost the only recommended method. The kinetics of oil shale pyrolysis and the influence of process conditions are of great importance as they can help researchers or engineers to predict the rate of decomposition as well as design efficient thermal decomposition reactors for engineering applications. The oil shale resource in the Jimsar oil shale mineralized belt, Xinjiang Province, China is about 1.15×10^{10} tons [1, 2]. Hence, it is necessary to study the kinetic parameters (the apparent activation energy (E), the pre-exponential factor (A) and the

* Corresponding author: e-mail *daifangqin@wust.edu.cn*

reaction mechanism function ($f(\alpha)$)) to predict the process of Jimsar oil shale pyrolysis. Various researches using thermogravimetric analysis (TGA) have been performed to study the effects of heating rate, temperature, particle size and processing data on the process of oil shale retorting [3–10]. According to the results, it is well known that the pyrolysis of oil shale can be divided into three stages: evaporation of free water, pyrolysis of organic matter and decomposition of inorganic minerals. Oil production takes place mainly in the second stage, pyrolysis of organic matter. As is known, the organic matter of oil shale mostly consists of bitumen and kerogen, the content and structure of which have been widely studied [11–13]. Bitumen, a term for nonpolymeric compounds, is soluble in common organic solvents and is a minor component; kerogen, which is the main component of oil shale organic matter, is insoluble in solvents due to its highly cross-linked macromolecular structure [14]. The process of oil shale pyrolysis is extremely complicated, because several competing or parallel reactions occur simultaneously, and various products are continuously generated and serve as new reactants. Many researchers have evidenced that there are more than two competing or parallel reactions in this stage. Li and Yue [15] developed a kinetic model of 11 parallel reactions, assuming that all the parallel reactions are first-order, and their apparent activation energies and apparent frequency factors are different. Bar et al. [16] assumed that there are three parallel first-order reactions in the pyrolysis process. Wang et al. [17] studied North-Korean oil shale, assuming that six parallel first-order reactions take place during the pyrolysis process. One obvious common point of these studies is that they consider each parallel reaction as a first-order reaction. Wang et al. [18] discovered that the pyrolysis process of oil shale could not be actually described by a simple first-order reaction. Moreover, the International Confederation for Thermal Analysis and Calorimetry (ICTAC) suggested that it should be better to separate the multi-steps entirely and analyze their kinetics individually [19]. In this paper, it is assumed that there are two parallel reactions in the devolatilization of organic matter, representing the volatilization of bitumen and pyrolysis of kerogen. The kinetic triplets of each reaction and the two stages are studied.

There are basically two kinds of methods for evaluating the kinetic triplets, model free methods and model fitting methods [19]. Model free methods, such as the Flynn-Wall-Ozawa (F-W-O) [20], Kissinger-Akahira-Sunose (K-A-S) [21] and Friedman [22] methods, assume that the reaction rate is only a function of temperature at constant conversion, therefore, the apparent activation energy is independent of the reaction mechanism [19]. In contrast, model fitting methods, such as Satave, Popescu and master plots methods [23–25], are capable of identifying multi-step reaction models suitable for the description of complex kinetics [19]. However, being based on a single heating rate value only, model fitting methods are considered unreliable.

In the present study, the multi-stage parallel reaction model is used to describe the decomposition of organic matter. The bi-Gaussian distribution

method [26] is adopted to fit the overlapping peak of TGA curves. For each reaction (subreactions and the total process reaction), E is calculated by the F-W-O, K-A-S and Friedman methods, and two master plots methods are adopted to obtain the reaction mechanism function.

2. Experimental

2.1. Oil shale samples

The oil shale used in this work was obtained from the Jimsar oil shale mineralized belt, Xinjiang Province, China. The raw samples were crushed and screened to 60 mesh size. The proximate and elemental analyses were performed according to the National Standards of China, as shown in Table 1. The dominant mineral phases of Jimsar oil shale identified are quartz, dolomite and a variety of clay minerals.

Table 1. Characteristics of Jimsar oil shale, wt%[a]

	Oil shale sample	Average	δ	Standard
Proximate analysis	Moisture	1.88	0.024	GB/T 212-2008
	Volatile matter	18.03	0.039	ISO 11722:1999
	Fixed carbon	3.15	0.021	ISO 1171:1997
	Ash	76.94	0.037	ISO 562:998
Elemental analysis	C	15.78	0.014	GB/T 476-2008
	H	2.55	0.025	GB/T 19227-2008
	O	4.54	0.021	GB/T 214-2007
	N	0.40	0.021	ISO 333:1996
	S	0.35	0.001	ISO 334:1992

[a] All the results are the mean of three experiments.
δ is the standard deviation of the three experiments.

2.2. Experimental procedure

The thermogravimetric analysis and differential thermal analysis (TGA/DTA) experiments were performed using a thermogravimetric (TG) analyzer (Netzsch STA 449C/6/MFC/G Jupiter). The samples were dried for 3 h at 101 °C under vacuum to remove free water before experiments. Approximately 20 mg of each oil shale sample was heated from room temperature to 1000 °C at heating rates of 1, 5, 10, 20 and 30 °C/min. The pyrolysis experiments were conducted in argon atmosphere and the purge gas flow rate of argon was 100 ml/min. The sample weight loss and the heat flow during the pyrolysis process were continuously recorded as a function of temperature and time by the TG analyzer.

3. Theory

3.1. Theoretical background and the apparent activation energy

The reaction rate of a solid-state reaction can be described as follows:

$$\frac{d\alpha}{dt} = Aexp\left(-\frac{E}{RT}\right)f(\alpha), \tag{1}$$

where $d\alpha/dt$ is the reaction rate, α is the reacted fraction, A is the pre-exponential factor, E is the apparent activation energy, R is the gas constant, T is temperature, and $f(\alpha)$ is the kinetic model.

Many differential equations based methods of calculating apparent activation energy can be obtained by different arrangements of Equation (1). As mentioned above, model free methods assume that the reaction rate is only a function of temperature at constant conversion, therefore, the apparent activation energy is independent of the reaction mechanism. In this work, the F-W-O, K-A-S and Friedman methods are used to calculate the apparent activation energy. Table 2 is a summary of these methods; by plotting the regression lines of Y vs X, the apparent activation energies can be obtained from the slopes.

Table 2. Summary of kinetic methods

Method	Approximated equation	X	Y
F-W-O	$\ln(\beta) = \ln\left(\frac{AE}{RG(\alpha)} - 5.331 - 1.052\frac{E}{RT}\right)$	$1/T$	$\ln(\beta)$
K-A-S	$\ln\left(\frac{\beta}{T^2}\right) = \ln\left(\frac{AR}{EG(\alpha)}\right) - \frac{E}{RT}$	$1/T$	$\ln\left(\frac{\beta}{T^2}\right)$
Friedman	$\ln\left(\beta\frac{\mathrm{d}\alpha}{\mathrm{d}T}\right) = \ln(Af(\alpha)) - \frac{E}{RT}$	$1/T$	$\ln\left(\beta\frac{d\alpha}{dT}\right)$

3.2. Kinetic mechanism

Master plots methods based on the differential and/or integral forms of Equation (1) employ reference theoretical curves which are characteristic curves independent of measurement conditions and can be easily obtained from experimental data. Recently, master plots methods have been successfully applied to analysis of solid-state reactions [7, 21, 27, 28]. Several master plots are always used together to distinguish the superimposed characteristic curves [27]. In this work, two master plots methods are employed to determine the kinetic model of Jimsar oil shale pyrolysis.

3.2.1. Master plots based on the integral form of kinetic data

The integration form of Equation (1) can be expressed as follows [7, 21]:

$$G(\alpha) = \int_0^{\alpha} \frac{d\alpha}{f(\alpha)} = \frac{A}{\beta}\int_{T_0}^{T} e^{-E/RT} dT = \frac{AE}{\beta R} p(u), \tag{2}$$

$$p(u) = \int_{\infty}^{u} -\left(\frac{e^{-u}}{u^2}\right) du, \tag{3}$$

$$u = E/RT, \tag{4}$$

where $p(u)$ is the temperature integral but has no analytical solution. In this work, the fourth rational approximation of Senum and Yang [28] is used to calculate the approximation of $p(u)$:

$$p(u) = \frac{x^3 + 18x^2 + 86x + 96}{x^4 + 20x^3 + 120x^2 + 240x + 120}. \tag{5}$$

The integral master plots formula for determining the kinetic model is:

$$\frac{G(\alpha)}{G(0.5)} = \frac{p(u)}{p(0.5)}. \tag{6}$$

The left side of Equation (6) can be calculated theoretically for a given α, while the right side of the equation can be obtained from experiment. If an appropriate kinetic model is used, the curves of $\frac{G(\alpha)}{G(0.5)}$ vs α and $\frac{p(u)}{p(0.5)}$ vs α should be coincident.

3.2.2. Master plots based on the integral and differential forms of kinetic data

The reaction mechanism function $f(\alpha)$ is proportional to the $y(\alpha)$ functions (Eq. (7)) by transforming the experimental TG data [23, 24]. Taking $\alpha = 0.5$ as a reference point, under non-isothermal conditions, the $y(\alpha)$ function can be expressed as follows:

$$y(\alpha) = \left(\frac{T}{T_{0.5}}\right)^2 \cdot \frac{\frac{d\alpha}{dt}}{\left(\frac{d\alpha}{dt}\right)_{0.5}} = \frac{f(\alpha)\cdot G(\alpha)}{f(0.5)\cdot G(0.5)}. \tag{7}$$

At the selected α, substituting the corresponding temperature T at different values of heating rate β into Equation (7), the plot of $\left(\frac{T}{T_{0.5}}\right)^2 \cdot \frac{\frac{d\alpha}{dt}}{\left(\frac{d\alpha}{dt}\right)_{0.5}}$ vs α can be drawn. And, for an arbitrary α, standard master plots of $\frac{f(\alpha)\cdot G(\alpha)}{f(0.5)\cdot G(0.5)}$ vs α can be obtained. In the same way, if a suitable kinetic model is used, the curves of $\left(\frac{T}{T_{0.5}}\right)^2 \cdot \frac{\frac{d\alpha}{dt}}{\left(\frac{d\alpha}{dt}\right)_{0.5}}$ vs α and $\frac{f(\alpha)\cdot G(\alpha)}{f(0.5)\cdot G(0.5)}$ vs α should be coincident.

Frequently-used mathematical expressions of $G(\alpha)$ and $f(\alpha)$ are summarized in Table 3.

Table 3. Some examples of kinetic models

	Reaction model	Code	$f(\alpha)$	$G(\alpha)$
1	One-dimensional diffusion	D_1	$-0.5\alpha^{-1}$	α^2
2	Two-dimensional diffusion	D_2	$[-\ln(1-\alpha)]^{-1}$	$(1-\alpha)\ln(1-\alpha)+\alpha$
3	Zhuravlev-Lesokin-Tempelman	D-ZLT_3	$\frac{3}{2}(1-\alpha)^{\frac{4}{3}}\left[(1-\alpha)^{-\frac{1}{3}}-1\right]^{-1}$	$\left[(1-\alpha)^{-1/3}-1\right]^2$
4	Jander diffusion	D-J_3	$6(1-\alpha)^{\frac{2}{3}}\left[1-(1-\alpha)^{\frac{1}{3}}\right]^{\frac{1}{2}}$	$\left[1-(1-\alpha)^{\frac{1}{3}}\right]^{\frac{1}{2}}$
5	Avarami-Erofeev	A_2	$2(1-\alpha)[-\ln(1-\alpha)]^{1/2}$	$[-\ln(1-\alpha)]^{1/2}$
6		A_3	$3(1-\alpha)[-\ln(1-\alpha)]^{2/3}$	$[-\ln(1-\alpha)]^{1/3}$
7		$A_{4/5}$	$\frac{4}{5}(1-\alpha)[-\ln(1-\alpha)]^{1/4}$	$[-\ln(1-\alpha)]^{5/4}$
8		$A_{5/6}$	$\frac{5}{6}(1-\alpha)[-\ln(1-\alpha)]^{1/5}$	$[-\ln(1-\alpha)]^{6/5}$
9	Mampel (first-order)	F_1	$1-\alpha$	$-\ln(1-\alpha)$
10	Second-order	F_2	$(1-\alpha)^2$	$(1-\alpha)^{-1}-1$
11	Third-order	F_3	$(1-\alpha)^3$	$-\frac{1}{2}(1-(1-\alpha)^{-2})$
12	Exponent power first-order	E_1	α	$\ln\alpha$
13	Exponent power second-order	E_2	0.5α	$\ln\alpha^2$
14	Contracting cylinder	R_2	$2(1-\alpha)^{\frac{1}{2}}$	$1-(1-\alpha)^{\frac{1}{2}}$
15	Contracting sphere	R_3	$(1-\alpha)^{\frac{2}{3}}$	$3\left[1-(1-\alpha)^{\frac{1}{3}}\right]$

3.3. The pre-exponential factor

With the determined apparent activation energy and kinetic model, the pre-exponential factor can be calculated by the following equation:

$$A = \frac{d\alpha/dt}{exp\left(-\frac{E}{RT}\right)*f(\alpha)}. \quad (8)$$

3.4. Multi-stage parallel reaction model

Oil of oil shale is mainly produced in the organic matter pyrolysis process, while many researchers have evidenced that there are more than two competing

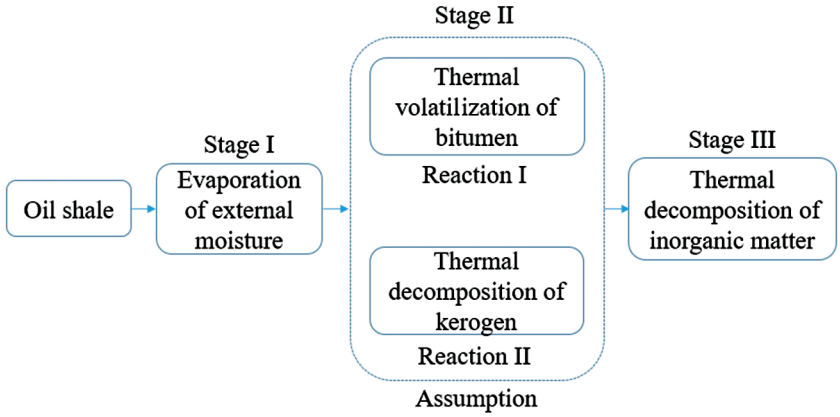

Fig. 1. The reaction route of the assumption model.

or parallel reactions in this stage. To predict the process of Jimsar oil shale pyrolysis, the kinetic model of each competing or parallel reaction should be identified. In this work, we think that the organic matter of oil shale is composed of two parts: kerogen and lower molecular weight bitumen, which is trapped into kerogen. Therefore, we assume that there are two parallel reactions in the organic matter pyrolysis process, one represents the volatilization of bitumen and the other represents the pyrolysis of kerogen. Figure 1 shows the reaction route of the assumption model. The multi-stage parallel reaction model considers the overall stage to be the result of combination of several independent pyrolysis reactions and neglects interactions between the reacting components [7, 19, 21]. Kinetic triplets for each reaction are calculated and the kinetic parameters for the overall pyrolysis process can be obtained by the weighted superposition method. The weighted factor is the ratio of mass loss of each parallel reaction to total mass loss.

In non-isothermal pyrolysis, the differential form of a kinetic equation for each reaction i can be expressed as:

$$\frac{d\alpha_i}{dT} = \frac{A_i}{\beta}\, exp\left(-\frac{E_i}{RT}\right) f_i(\alpha_i). \tag{9}$$

The weighted factor of each reaction can be obtained by Equations (10) and (11):

$$r_i = \frac{m_{io} - m_{if}}{m_o - m_f}, \tag{10}$$

$$\sum_1^m r_i = 1, \tag{11}$$

where m_{io} and m_{if} are the initial and final masses of reaction i, respectively; m_o and m_f are the initial and final masses of the sample, respectively; m is the number of reactions, in this study, $m = 2$.

The conversion rate and the apparent activation energy of the overall pyrolysis process can be obtained by:

$$\alpha = \frac{m_o - m_T}{m_o - m_f} = \sum_{i=1}^m (r_i \alpha_i), \tag{12}$$

$$E = \sum_{i=1}^{m}(r_i E_i), \tag{13}$$

where m_T is the sample mass at temperature T and r_i is the weight factor.

3.5. Separation of overlapping peaks

Peaks in the DTG curve represent the main weightlessness stages in the pyrolysis process of oil shale and result from several competing or parallel reactions. For example, we assume that in the 2nd stage of weightlessness, there are two parallel reactions, therefore, the peak representing this stage should be the superposition of two subpeaks.

The multi-peak fitting method is suitable for separating the overlapping peaks of the DTG curve into numerous subpeaks, which can represent the physical characteristics of the reaction.

When the difference between the experimental and fitted data (SS) is minimum, the subpeaks can be considered to be the most representative:

$$SS = \sum_{i=1}^{n} r_i[y_i - f_i(x_i; P)]^2, \tag{14}$$

where n is the number of iterations, P is the matrix with three parameters: height, position and full width at half maximum (FWHM) of the peak.

Generally, in the Gaussian method, subpeaks are symmetrical, and the fitting accuracy is not as high as in the bi-Gaussian method [7, 21]. In this work, the bi-Gaussian multi-peak fitting method is used to separate the overlapping peaks of DTG curves. This method modifies the f_i function (Eq. (14)) to correctly fit the peaks [29, 30]:

$$f_i = \begin{cases} Hexp[-(x_i - x_c)^2/2\sigma_1^2] & x_i < x_c \\ Hexp[-(x_i - x_c)^2/2\sigma_2^2] & x_i > x_c \end{cases}, \tag{15}$$

where H is the height of peak, σ_1 is the left FWHM, σ_2 is the right FWHM, and $\sigma_1 \neq \sigma_2$.

To assess the quality of the multi-peak fitting (QOF), Equation (16) takes into account the differences between model and experimental values. The lower the QOF, the better the fitting quality:

$$QOF\% = 100 \times \frac{\sqrt{\sum_{i=1}^{n_d}\left[\left(\frac{d\alpha}{dt}\right)_{cal} - \left(\frac{d\alpha}{dt}\right)_{exp}\right]^2/n_d}}{\frac{d\alpha}{dt}_{max.exp}}, \tag{16}$$

where n_d is the data number, $(d\alpha/dt)_{cal}$ and $(d\alpha/dt)_{exp}$ are the calculated and experimental TG curves, respectively, $(d\alpha/dt)_{max,exp}$ stands for the maximum experimental data.

4. Results and discussion

4.1. Analysis of pyrolysis process

Figure 2 depicts the TG curves of Jimsar oil shale pyrolysis as a function of temperature at heating rates of 1, 5, 10, 20 and 30 °C/min. It can be seen that at different heating rates, the sample exhibits similar pyrolysis characteristics and the total pyrolysis process can be divided into three basic stages [4, 7, 10, 17, 18, 21]. Stage I is the lower temperature region (< 200 °C) in which the weight loss is attributed to the evaporation of external moisture and interlayer water from clay minerals, the weight loss in this stage is about 5%. In stage II, in the medium temperature range of 200–550 °C, due to the decomposition of organics, the weight loss is about 70% of total. In stage III, from 550 to 950 °C, the final weight loss is mostly assigned to the thermal decomposition of inorganic minerals, such as calcite, ankerite, dolomite, etc.

Figure 3 shows the DTG curves of Jimsar oil shale pyrolysis with two distinct peaks corresponding to stage II and stage III, respectively. The figure reveals that the maximum peak value and the corresponding temperature increase with increasing heating rate. This is generally because the temperature gradient of the oil shale particle increases with increasing heating rate. Granoff and Nuttall Jr [31], Shin and Sohn [32], and Pan et al. [33] developed different mathematical models to predict the inner temperature and temperature gradient

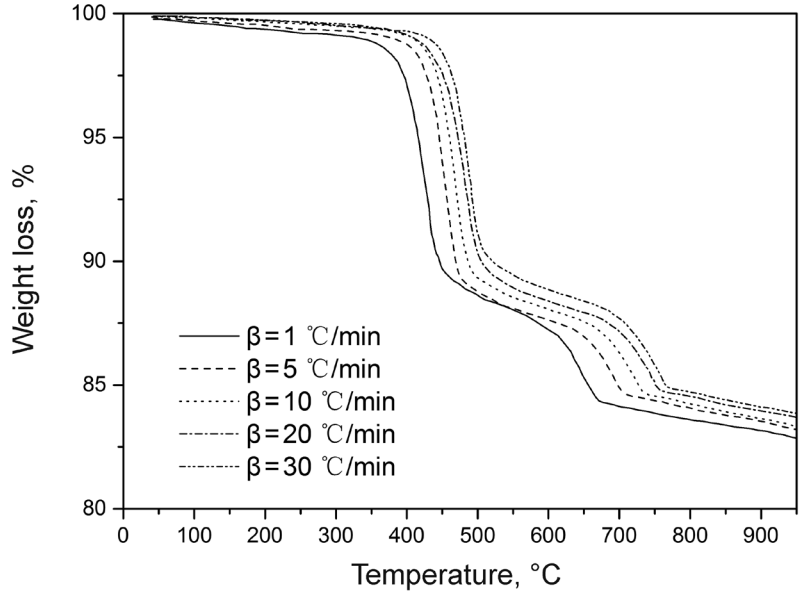

Fig. 2. Weight loss curves of Jimsar oil shale.

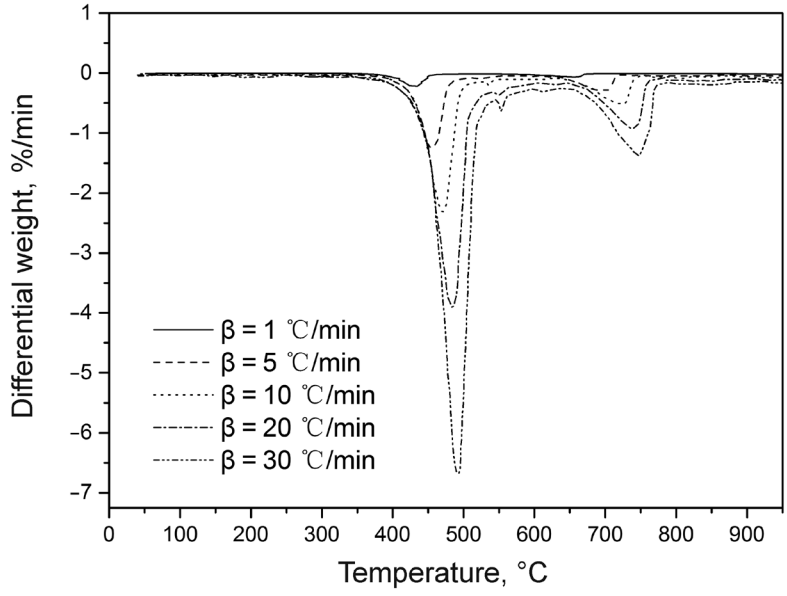

Fig. 3. Differential weight loss curves of Jimsar oil shale.

of a single oil shale particle. The increase of temperature gradient strengthens the inertia effect of devolatilization and affects the decomposition of the inner part of the oil shale particle, and then increases the T_{max} temperature. Moreover, at high heating rate, products are generated faster than at low heating rate, and the diffusion rate of products affects the pyrolysis process [34, 35]. This work focuses on stages II and III of oil shale pyrolysis as the main research objects.

4.2. Kinetic triplets of Jimsar oil shale pyrolysis

In the current work, the bi-Gaussian fitting method is adopted to separate the overlapping peaks of DTG curves. In stage II, the peak of the DTG curve at each heating rate is separated into two subpeaks. In stage III, which, as is known, is mainly the thermal decomposition of inorganic minerals, the peak of the DTG curve is fitted by only one peak.

Figure 4 and Figure 5 show the curves of the bi-Gaussian multi-peak fitting of Jimsar oil shale pyrolysis. It is indicated that the QOFs of stages II and III of the process are within the acceptable range. The areas under the peaks are integrated to determine the amount of weightlessness of each reaction [10, 21]. In stage II (Fig. 4), the weight loss proportion of the first subreaction (reaction I) representing bitumen volatilization is about 12–15% in the temperature range of 350–500 °C. The second subreaction of stage II (reaction II), which accounts for 85–88% of the whole stage, represents the pyrolysis of kerogen. From Figure 4 it can be seen that the two reactions occur almost at the same time, while the share of reaction I is small (Table 4). Moreover, the temperature

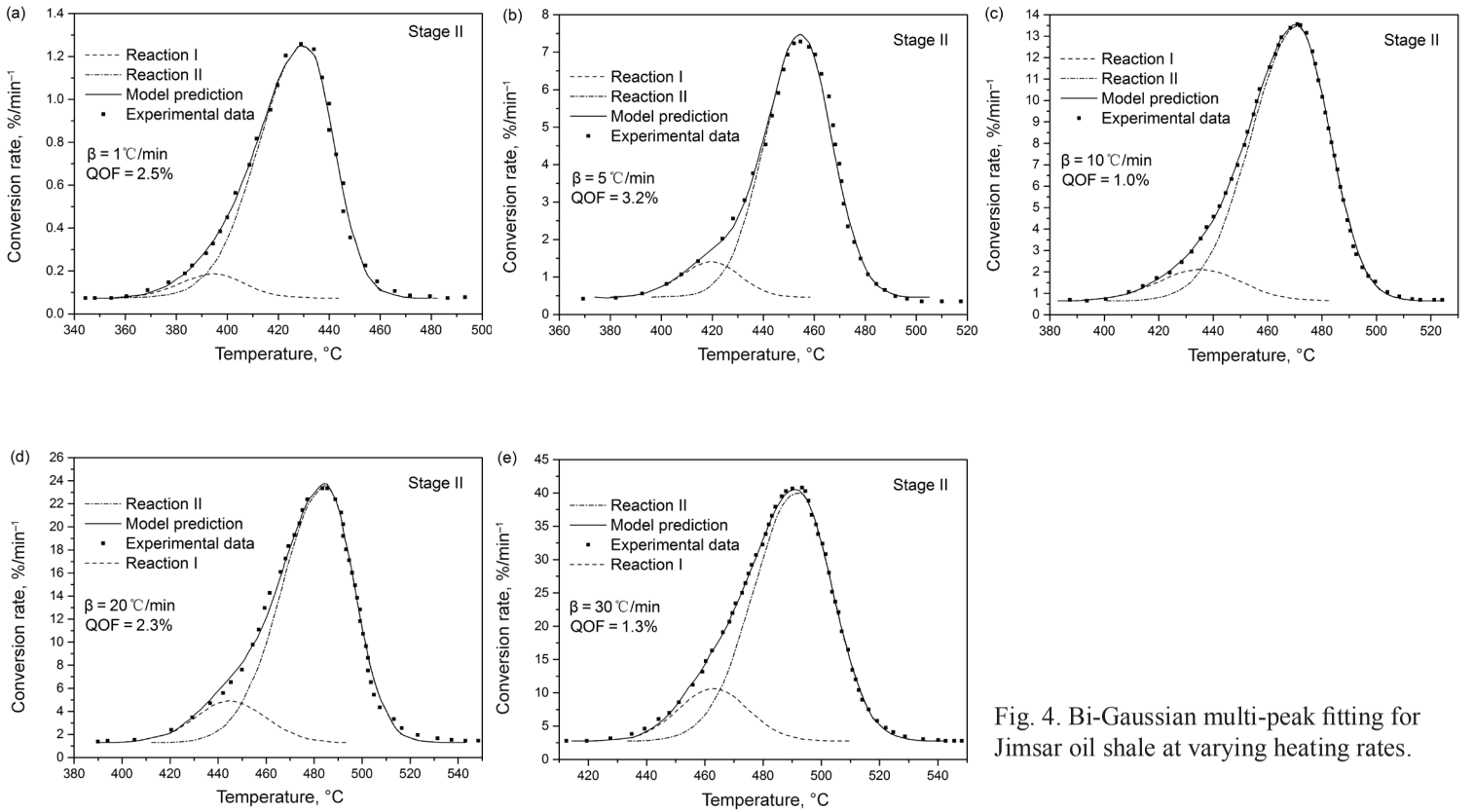

Fig. 4. Bi-Gaussian multi-peak fitting for Jimsar oil shale at varying heating rates.

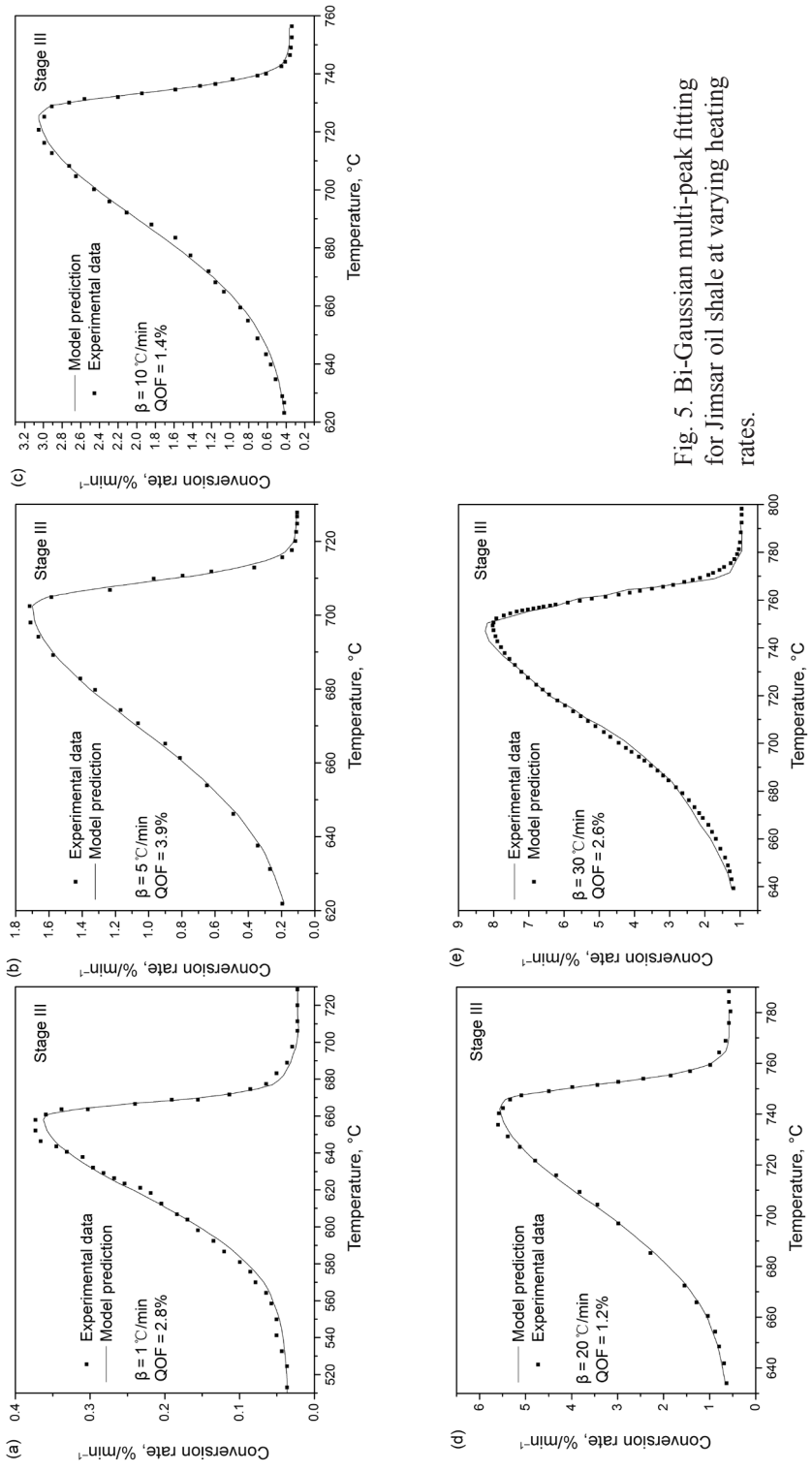

Fig. 5. Bi-Gaussian multi-peak fitting for Jimsar oil shale at varying heating rates.

Table 4. Kinetic triplets of subreactions for stage II and stage III

Stage I		β T_{max}	Bi-Gaussian		E^a	Mechanism				ln$A$
			MLP[b]		Eq. (14)	R	Eq. (15)	R		
Stage II	Reaction I	1	394	7.6	200 ± 16	F_2	0.9835	F_2	0.9864	35.78 ± 1
		5	419	10.8			0.9868		0.9873	36.54 ± 4
		10	435	10.8			0.9832		0.9852	36.17 ± 1
		20	445	13.6			0.9865		0.9815	38.89 ± 3
		30	463	15.7			0.9789		0.9847	36.53 ± 1
	Reaction II	1	429	92.4	220 ± 14	R_3	0.9883	D-ZLT_3	0.9867	36.85
		5	455	89.2			0.9854		0.9768	37.15 ± 4
		10	471	89.2			0.9788		0.9877	37.00 ± 4
		20	484	86.4			0.9768		0.9676	37.03 ± 4
		30	492	84.3			0.9839		0.9748	36.94 ± 5
	Total	1	429		227.8 ± 8	F_1	0.9857	A_n, F_1	0.9859	39.97 ± 1
		5	455				0.9784		0.9816	40.27 ± 1
		10	471				0.9779		0.9873	40.12 ± 1
		20	484				0.9867		0.9884	40.12 ± 1
		30	492				0.9879		0.9858	40.15 ± 1
Stage III		1	658		242 ± 24	R_2	0.9861	R_2	0.9867	30.26 ± 3
		5	702				0.9542		0.9863	30.2
		10	725				0.9678		0.9847	30.22 ± 1
		20	742				0.9786		0.9858	30.28 ± 1
		30	750				0.9847		0.9876	30.40 ± 1

[a] Calculated using the Friedman equation, kJ/mol.
[b] The mass loss percent of each reaction, %.

ranges of two subreactions increase with increasing heating rate, and the T_{max} values of these reactions rise steadily. This is caused by the inner temperature gradient of the oil shale particle.

In stage III (Fig. 5), with increasing heating rate, the T_{max} of the decomposition of inorganic minerals grows steadily. Similarly to stage II, the temperature ranges of stage III also increase with increasing heating rate and the T_{max} values of its reactions increase steadily.

Based on Figure 4 and Figure 5, the kinetic triplets of each subreaction and the total stage can be calculated using the theories mentioned above (Table 4).

Figure 6 shows the *E* values for stage II calculated by the Friedman, F-W-O and K-A-S methods. The figure reveals that the *E* values of reactions I and II and the total stage II increase slightly with increasing α, while the *E* of reaction I is lower than that of reaction II. Figure 6 also demonstrates that the *E* of the total stage II is similar to the respective value of reaction II, which means that the latter reaction is prevailing in stage II. Figure 6d depicts the decrease of *E* values calculated by three different methods. It can be seen that F-W-O and K-A-S provide similar *E*, yet lower than that found by the Friedman method.

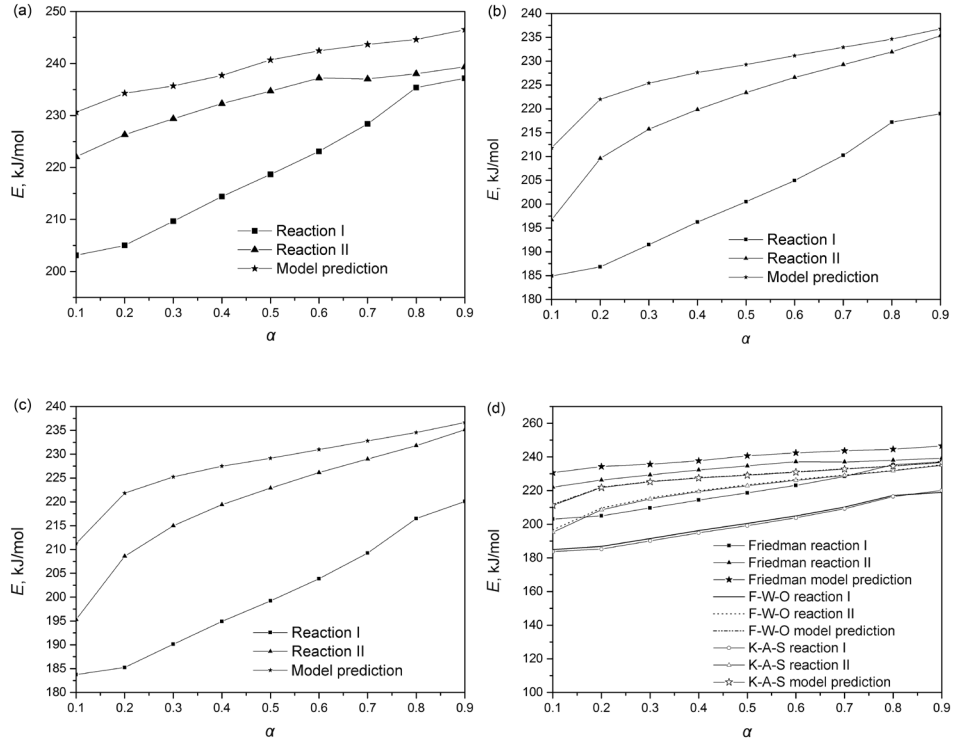

Fig. 6. *E* of stage II calculated by different methods vs α: (a) *E* calculated by the Friedman method, (b) *E* calculated by F-W-O, (c) *E* calculated by K-A-S, (d) comparison of *E* calculated by the three methods.

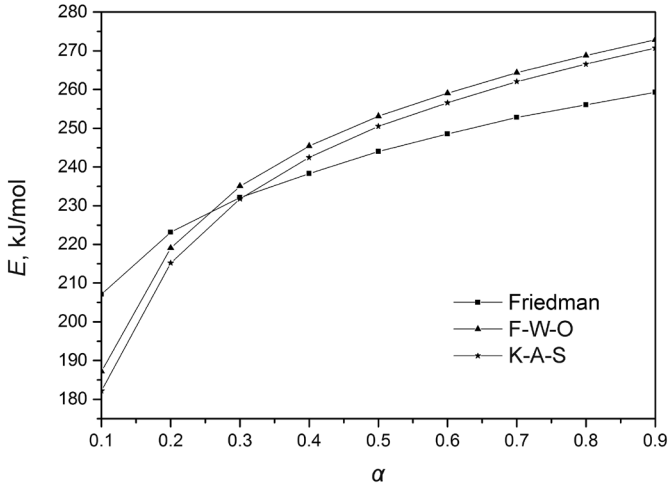

Fig. 7. E of stage III calculated by Friedman, F-W-O and K-A-S methods vs α.

This is because the latter method uses numerical differentiation that may lead to inaccurate rate data, also when smoothing noisy data [19].

Figure 7 depicts the curves of E vs α of stage III. It is revealed that F-W-O and K-A-S afford similar E values which slightly increase with increasing α.

Based on the results illustrated in Figure 4 and Figure 5, two master plots methods are used to analyze the peaks, the results are shown in Figure 8 and Table 4. From Figure 8 it can be seen that for each process stage the experimental data correspond to one of the predicted theoretical model curves closely, which means that the pyrolysis mechanism does not change with changing heating rate. The difference in the experimental values obtained at different heating rates may be caused by the difference in temperature gradient between the central part and the surface of the oil shale particle. Each theoretical prediction model corresponds to a reaction model which reveals the inherent property and relationship between the extent and temperature of oil shale pyrolysis. From Figures 8a and 8e it can be concluded that reaction I of stage II follows the F_2 model. At the same time, for reaction II of stage II, a different method gives a different theoretical prediction model which is different from the one depicted in Figure 8b, while the experimental data correspond to the R_3 model obtained by the master plots method on the basis of the integral form of Equation (14). In contrast, Figure 8f shows the D-ZLT$_3$ model obtained by the master plots method on the basis of the integral and differential forms of Equation (15). The experimental data for the total stage II comply with the F_1 model calculated by Equation (14) (Fig. 8c) and A_n fits the one obtained by Equation 15) (Fig. 8g). Figures 8d and 8h expose that the decomposition process of inorganic minerals in stage III can be described by the R_2 model. Different methods are mutually complementary rather than exclusive. Varying results for reaction II of stage II are mainly due to theory difference between the methods.

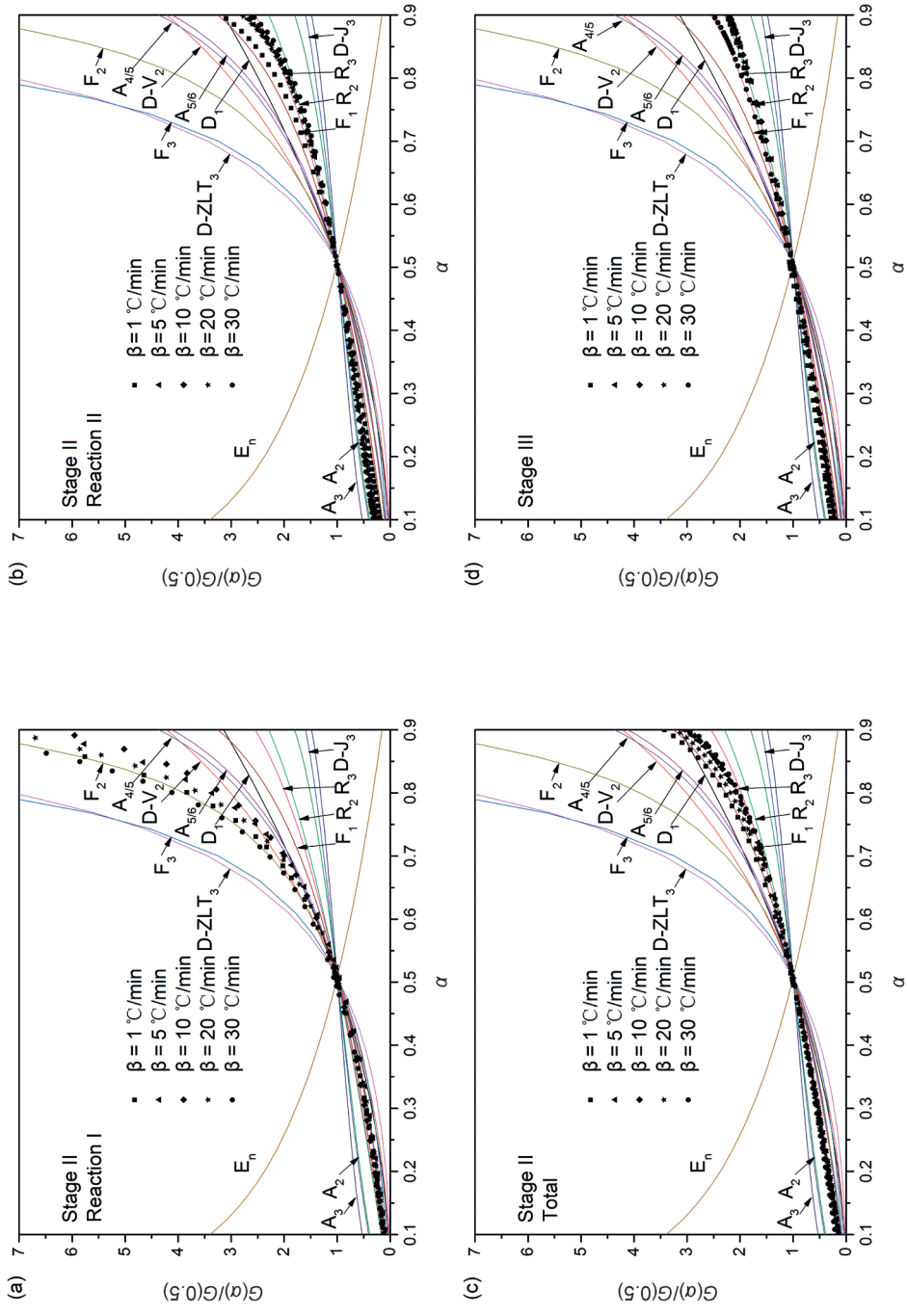
(a)
Stage II
Reaction I
β = 1 ℃/min
β = 5 ℃/min
β = 10 ℃/min
β = 20 ℃/min
β = 30 ℃/min
D-ZLT3
E_n
A3 A2
F1 R2 R3 D-J3
D1
A5/6
F3
D-V2
A4/5
F2
G(α)/G(0.5)
α
(b)
Stage II
Reaction II
(c)
Stage II
Total
(d)
Stage III

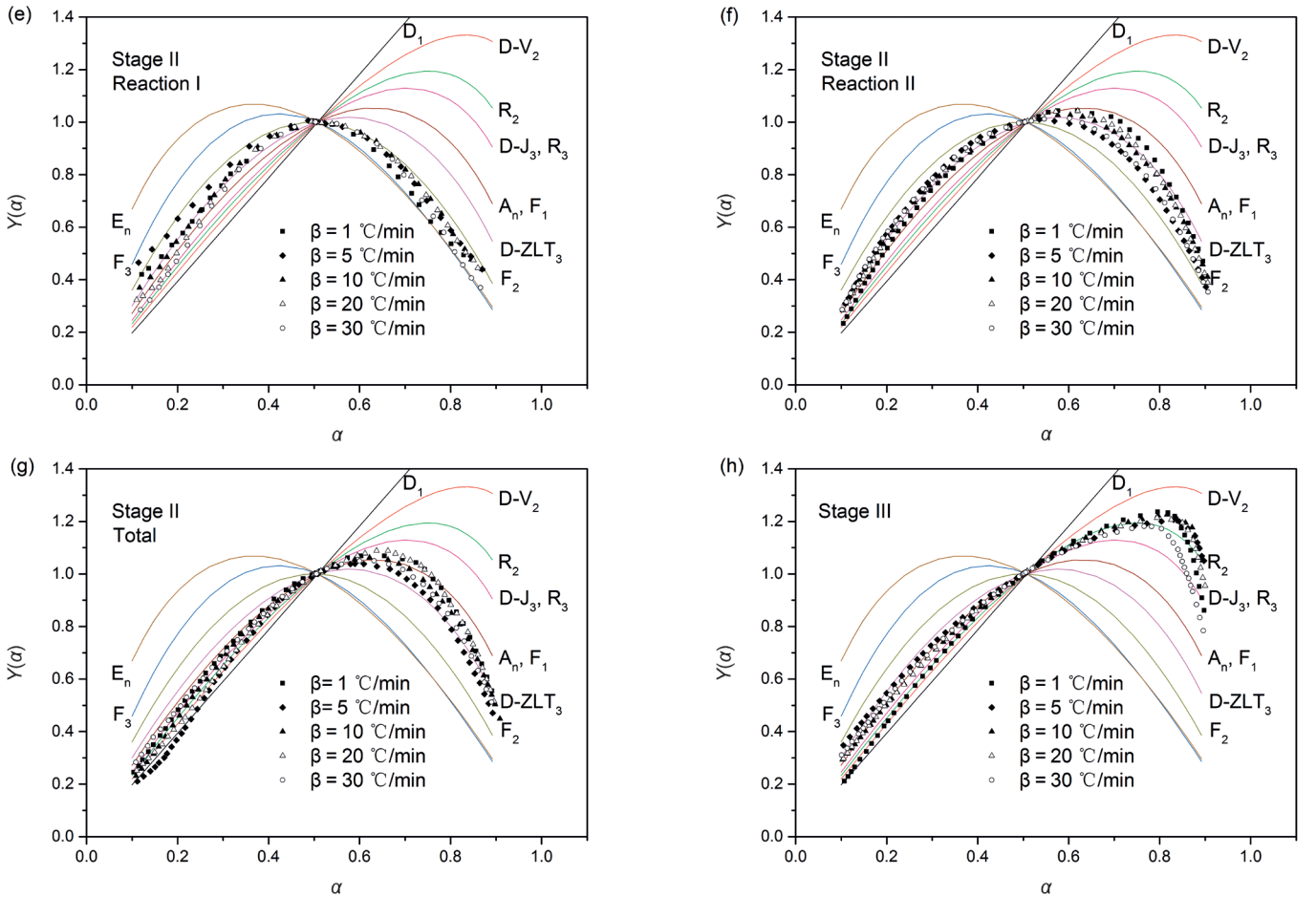

Fig. 8. Experimental and standard y(α) plots calculated by Equation (14) ((a)–(d)) and Equation (15) ((e–h)).

Table 4 presents the kinetic triplets of Jimsar oil shale pyrolysis and the reaction models of stage II and stage III.

From Figure 2, Figure 3, Figure 8 and Table 4 it can be seen that at different heating rates, the samples exhibit similar pyrolysis characteristics, and the mechanism of pyrolysis does not change with changing heating rate. At the same time, due to the difference in temperature gradient between the central part and the surface of the oil shale particle, as well as in diffusion rate between the products at different heating rates, the experimental values obtained at different heating rates may also differ. Therefore, it can be concluded that heating rate exerts little influence on individual kinetic parameters but has some impact on the pyrolysis process as a whole.

5. Conclusions

The pyrolysis process of Jimsar oil shale can be divided into three stages. In stage I, the weight loss is attributed to the evaporation of external moisture and interlayer water from clay minerals (< 200 °C), the weight loss of this stage is about 5%. In stage II, in the medium temperature range of 200–550 °C, due to the decomposition of organics, the weight loss is about 70% of total. In stage III, in the temperature range of 550–950 °C, the final weight loss is mostly attributed to the thermal decomposition of inorganic minerals. Based on the bi-Gaussian fitting method, stage II can be described by two subpeaks, one represents the volatilization of bitumen and the other represents the pyrolysis of kerogen. The average activity energies of reaction I and reaction II of stage II are 200 kJ/mol and 220 kJ/mol, respectively. For the total stage II and stage III, the average activity energies are 227.8 kJ/mol and 242 kJ/mol, respectively. The reaction models for reaction I of stage II is F_2, reaction II of stage II can be described by both the R_3 and D-ZLT_3 models according to different master plots methods. The total reaction model for stage II follows the F_1 model. For stage III, the decomposition of inorganic minerals can be described by the R_2 model. According to the results, heating rate exerts little influence on individual kinetic parameters but has some impact on the pyrolysis process as a whole. It can be proved that the multi-stage parallel reaction model can be effectively used to study solid fuel pyrolysis. We anticipate that this work can provide useful information for the study and production of Jimsar oil shale.

Acknowledgements

This work was supported by the Key Laboratory for Ferrous Metallurgy and Resources Utilization of Ministry of Education of Wuhan Science and Technology, Wuhan, China (Grant No. FMRU201502).

REFERENCES

1. Qian, J. L., Yin, L, Wang, J. Q., Li, S. Y., Han, F., He, Y. G. *Oil Shale* – Petroleum Alternative. China Petrochemical Press, Beijing, 2010.
2. Bai, Y. L. Prospects for development of oil shale deposits in southeastern margin of Junggar basin. *Xinjiang Petroleum Geology,* 2008, **29**(4), 462–465 (in Chinese).
3. Williams, P. T., Ahmad, N. Investigation of oil-shale pyrolysis processing conditions using thermogravimetric analysis. *Appl. Energ.,* 2000, **66**(2), 113–133.
4. Bojan, J. The kinetic modeling of the non-isothermal pyrolysis of Brazilian oil shale: Application of the Weibull probability mixture model. *J. Petrol. Sci. Eng.*, 2013, **111**, 25–36.
5. Liu, Q. Q., Han, X. X., Li, Q. Y., Huang, Y. R., Jiang, X. M. TG–DSC analysis of pyrolysis process of two Chinese oil shales. *J. Therm. Anal. Calorim.,* 2014, **116**(1), 511–517.
6. Moine, E. C., Tangarfa, M., Khachani, M., El Hamidi, A., Halim, M., Arsalane, S. Thermal oxidation study of Moroccan oil shale: A new approach to non-isothermal kinetics based on deconvolution procedure. *Fuel*, 2016, **180**, 529–537.
7. Wang, Q., Jia, C. X., Jiang, Q. Q., Wang, Y., Wu, D. Y. Pyrolysis model of oil sand using thermogravimetric analysis. *J. Therm. Anal. Calorim.*, 2014, **116**(1), 499–509.
8. Al-Harahsheh, M., Al-Ayed, O., Robinson, J., Kingman, S., Al-Harahsheh, A., Tarawneh, K., Saeid, A., Barranco, R. Effect of demineralization and heating rate on the pyrolysis kinetics of Jordanian oil shales. *Fuel Process. Technol.*, 2011, **92**(9), 1805–1811.
9. Tiwari, P., Deo, M. Detailed kinetic analysis of oil shale pyrolysis TGA data. *AIChE J.,* 2012, **58**(2), 505–515.
10. Pan, L. W., Dai, F. Q., Li, G. Q., Liu, S. A TGA/DTA-MS investigation to the influence of process conditions on the pyrolysis of Jimsar oil shale. *Energy*, 2015, **86**, 749–757.
11. Singleton, M. F., Burnham, A. K., Richardson, J. H., Clarkson, J. E. Biomarkers in oil shale: occurrence and applications. *Symposium on Geochemistry and Chemistry of Oil Shale Presented before the Divisions of Fuel Chemistry, Geochemistry and Petroleum Chemistry, Inc.* American Chemical Society Seattle Meeting, March 20–25, 1983, 181–194.
12. Brassell, S. C., Eglinton, G., Sheng, G. Y., Fu, J. M. Biological markers in lacustrine Chinese oil shales. *Geol. Soc. Spec. Publ.*, 1988, **40**, 299–308.
13. Wei, X. C., Liu, S. C., Xia, M. The genesis analysis of oil shale in southern Jimisar, Xinjiang. *Xinjiang Geology,* 2012, **30**, 66–70 (in Chinese, with English abstract).
14. Oja, V. Examination of molecular weight distributions of primary pyrolysis oils from three different oil shales via direct pyrolysis Field Ionization Spectrometry. *Fuel,* 2015, **159**,759–765.
15. Li, S. Y., Yue, C. T. Study of pyrolysis kinetics of oil shale. *Fuel*, 2003, **82**(3),

337–342.
16. Bar, H., Ikan, R., Aizenshtat, Z. Comparative study of the isothermal pyrolysis kinetic behavior of some oil shales and coals. *J. Anal. Appl. Pyrol.,* 1988, **14**(1), 49–71.
17. Wang, W., Li, S. Y., Li, L. Y., Ma, Y., Yue, C. T., He, J. L. Pyrolysis kinetics of North-Korean oil shale. *Oil Shale*, 2014, **31**(3), 250–265.
18. Wang, Q., Liu, H. P., Sun, B. Z., Li, S. H. Study on pyrolysis characteristics of Huadian oil shale with isoconversional method. *Oil Shale*, 2009, **26**(2), 148–162.
19. Vyazovkin, S., Burnham, A. K., Criado, J. M., Pérez-Maqueda, L. A., Popescu, C.-M., Sbirrazzuoli, N. ICTAC Kinetics Committee recommendations for performing kinetic computations on thermal analysis data. *Thermochim. Acta*, 2011, **520**, 1–19.
20. Flynn, J. H., Wall, L. A. A quick, direct method for the determination of activation energy from thermogravimetric data. *J. Polym. Sci., Part C: Polym. Lett.,* 1966, **4**(5), 323–328.
21. Bai, F. T., Guo, W., Lü, X. S., Liu, Y. M., Guo, M. Y., Li, Q., Sun, Y. H. Kinetic study on the pyrolysis behavior of Huadian oil shale via non-isothermal thermogravimetric data. *Fuel*, 2015, **146**, 111–118.
22. Friedman, H. L. Kinetics of thermal degradation of char-forming plastics from thermogravimetry. Application to a phenolic plastic. *J. Polym. Sci. Part C: Pol. Sym.,* 1964, **6**(1), 183–195.
23. Criado, J. M., Malek, J., Ortega, A. Applicability of the master plots in kinetic analysis of non-isothermal data. *Thermochim. Acta*, 1989, **147**(2), 377–385.
24. Malek, J. The kinetic analysis of non-isothermal data. *Thermochim. Acta*, 1992, **200**, 257–269.
25. Gotor, F. J., Criado, J. M., Malek, J., Koga, N. Kinetic analysis of solid-state reactions: the universality of master plots for analyzing isothermal and nonisothermal experiments. *J. Phys. Chem. A*, 2000, **104**(46), 10777–10782.
26. Zhu, K. H., Wan, Y. J. Gauss function method for DTA overlapping peak. *Computers and Applied Chemistry,* 1997, 4, 303–306 (in Chinese with English abstract).
27. Criado, J., Malek, J., Ortega, A. Applicability of the master plots in kinetic analysis of non-isothermal data. *Thermochim. Acta*, 1989, **147**(2), 377–385.
28. Senum, G. I., Yang, R. T. Rational approximations of the intergral of the Arrhenius function. *J. Therm. Analysis*, 1977, **11**(3), 445–447.
29. Romanenko, S. V., Stromberg, A. G. Classification of mathematical models of peak-shaped analytical signals. *J. Anal. Chem+.,* 2000, **55**(11), 1024–1028.
30. Romanenko, S. V., Stromberg, A. G. Modelling of analytical peaks: peaks modifications. *Anal. Chim. Acta,* 2007, **581**(2), 343–354.
31. Granoff, B., Nuttall Jr, H. E. Pyrolysis kinetics for oil-shale particles. *Fuel*, 1977, **56**(3), 234–240.
32. Shin, S. M., Sohn, H. Y. A mathematical model for the retorting of a large block of oil shale: effect of the internal temperature gradient. *Fuel*, 1978, **57**(10), 622–630.

33. Pan, Z. L., Feng, H. Y., Smith, J. M. Rates of pyrolysis of Colorado oil shale. *AIChE J.*, 1985, **31**(5), 721–728.
34. Williams, P. T., Ahmad, N. Investigation of oil-shale pyrolysis processing conditions using thermogravimetric analysis. *Appl. Energ.*, 2000, **66**(2), 113–133.
35. You, Y. H., Huang, H., Shao, G. W., Hu, J., Xu, X. C., Luo, X. B. A three-dimensional numerical model of unsteady flow and heat transfer in ceramic honeycomb regenerator. *Appl. Therm. Eng.*, 2016, **108**, 1243–1250.

Presented by V. Oja
Received August 28, 2019